

# Aerial Active STAR-RIS-assisted Satellite-Terrestrial Covert Communications

Chuang Zhang<sup>1b</sup>, Geng Sun<sup>1b</sup>, *Senior Member, IEEE*, Jiahui Li<sup>1b</sup>, Jiacheng Wang<sup>1b</sup>, Ruichen Zhang<sup>1b</sup>,  
Dusit Niyato<sup>2b</sup>, *Fellow, IEEE*, Shiwen Mao<sup>1b</sup>, *Fellow, IEEE*, and Tony Q. S. Quek<sup>1b</sup>, *Fellow, IEEE*

**Abstract**—An integration of satellites and terrestrial networks is crucial for enhancing performance of next generation communication systems. However, the networks are hindered by the long-distance path loss and security risks in dense urban environments. In this work, we propose a satellite-terrestrial covert communication system assisted by the aerial active simultaneous transmitting and reflecting reconfigurable intelligent surface (AASAR-RIS) to improve the channel capacity while ensuring the transmission covertness. Specifically, we first derive the minimal detection error probability (DEP) under the worst condition that the Warden has perfect channel state information (CSI). Then, we formulate an AASAR-RIS-assisted satellite-terrestrial covert communication optimization problem (ASCCOP) to maximize the sum of the fair channel capacity for all ground users while meeting the strict covert constraint, by jointly optimizing the trajectory and active beamforming of the AASAR-RIS. Due to the challenges posed by the complex and high-dimensional state-action spaces as well as the need for efficient exploration in dynamic environments, we propose a generative deterministic policy gradient (GDPG) algorithm, which is a generative deep reinforcement learning (DRL) method to solve the ASCCOP. Concretely, the generative diffusion model (GDM) is utilized as the policy representation of the algorithm to enhance the exploration process by generating diverse and high-quality samples through a series of denoising steps. Moreover, we incorporate an action gradient mechanism to accomplish the policy improvement of the algorithm, which refines the better state-action pairs through the gradient ascent. Simulation results demonstrate that the proposed approach significantly outperforms important benchmarks, and also validate the performance and practicality under different algorithm parameters and environment settings.

**Index Terms**—Active STAR-RIS, Covert Communications, Satellite-Terrestrial Fair Communications, Deep Reinforcement

Chuang Zhang is with the College of Computer Science and Technology, Jilin University, Changchun 130012, China, and also with the Singapore University of Technology and Design, Singapore 487372 (email: chuangzhang1999@gmail.com).

Geng Sun is with the College of Computer Science and Technology, Jilin University, Changchun 130012, China, and also with the College of Computing and Data Science, Nanyang Technological University, Singapore 639798 (e-mail: sungeng@jlu.edu.cn).

Jiahui Li is with the College of Computer Science and Technology, Jilin University, Changchun 130012, China, and also with the Key Laboratory of Symbolic Computation and Knowledge Engineering of Ministry of Education, Jilin University, Changchun 130012, China (e-mail: lijiahui0803@foxmail.com).

Jiacheng Wang, Ruichen Zhang and Dusit Niyato are with the College of Computing and Data Science, Nanyang Technological University, Singapore 639798 (e-mails: jiacheng.wang@ntu.edu.sg, ruichen.zhang@ntu.edu.sg, dniyato@ntu.edu.sg).

Shiwen Mao is with the Department of Electrical and Computer Engineering, Auburn University, Auburn, AL 36849, USA (e-mail: smao@ieee.org).

Tony Q. S. Quek is with the Information System Technology and Design Pillar, Singapore University of Technology and Design, Singapore 487372 (e-mail: tonyquek@sutd.edu.sg).

(Corresponding author: Geng Sun and Jiahui Li.)

Learning, Generative Diffusion Model

## I. INTRODUCTION

As a crucial component of the sixth-generation (6G) wireless communication systems, satellite-terrestrial communications have garnered significant attention in both military and civil sectors due to their extensive coverage and long-distance transmission capabilities [1]. For instance, in the aftermath of natural disasters such as earthquakes and floods, satellite-terrestrial systems can be an indispensable solution to re-establish communication links with disabled ground-based facilities. However, the persistent challenges of high path loss from the long-distance transmission and extreme penetration loss caused by obstacles continue to affect the performance of these systems, especially in dense urban environments [2].

In such cases, low-altitude economy (LAE) offers new opportunities for the development of satellite-terrestrial communications [3]. As the core supporters of LAE, low-altitude platforms (LAPs), e.g. unmanned aerial vehicles (UAVs), can be deployed as the aerial relay nodes between satellites and ground users. Compared to the fixed relay communication mode, LAP-based aerial relay communications can bring an additional degree of freedom by dynamically adjusting their trajectories, thereby improving the channel capacity for the users in various locations. While the high line-of-sight (LoS) probability of air-to-ground channels improves the transmission performance, the inherent broadcast nature of wireless communications simultaneously heightens the security vulnerabilities [4]. As such, two widely used conventional techniques for ensuring secure communications are the encryption method in the high-layer network protocol stack and physical layer security [5]. However, these methods cannot fundamentally address security threats of satellite-terrestrial communications, particularly in the scenarios involving advanced technologies such as quantum computers, which could potentially break the conventional encryption methods, and more intelligent adversaries that may adapt to exploit emerging decoding techniques [6].

Given the limitations of conventional security methods in addressing new forms of threats, covert communications have been recognized as a promising alternative [7]. Specifically, covert communications exploit the uncertainty of the Warden to prevent it from detecting the transmission by hiding the transmission information in noise, thereby providing a higher-level communication security. This approach aligns well with the dynamic capabilities of reconfigurable intelligent surfaces

(RIS) and their variants, which adjust wireless channels by controlling intelligent reflection elements, thus positioning them as crucial technologies in covert communications for terrestrial environments [6]. Among the available RIS solutions, the active simultaneously transmitting and reflecting RIS (STAR-RIS) can become the preferred choice for mounting on LAPs in the satellite-terrestrial covert communication systems. This is because it can not only achieve the full-space coverage by a horizontal mounting mode, but also enhance the transmission rate under varying and complex channel conditions by actively amplifying and concentrating the wireless signal in the desired direction. Therefore, this paper aims to explore the satellite-terrestrial covert communications with the aid of the aerial active STAR-RIS (AASTAR-RIS).

### A. Prior Works

We review related works from three aspects, including the architecture of satellite-terrestrial covert communications, uncertainty sources and performance metrics in satellite-terrestrial covert communications, and optimization methods for satellite-terrestrial covert communications, which motivates us to contribute this work.

1) *Architecture of Satellite-Terrestrial Covert Communications*: Existing works in the architecture of satellite-terrestrial covert communications can be mainly divided into direct mode and relay mode. For the direct mode, Zhang *et al.* [8] investigated an ultra-dense low Earth orbit (LEO) satellite downlink system, where the sidelobe leakages of other satellites are utilized to ensure the covertness. In [9], the authors developed a direct satellite-terrestrial downlink system by employing the rate-splitting multiple access technique to transmit jamming signals. However, this mode typically overlooks the long-distance path loss and complex propagation environments between satellites and ground users, which are particularly problematic in dense urban areas. In terms of the relay mode, Wu *et al.* [10] studied the ground device-based satellite-terrestrial covert relay communications, where multiple ground base stations are randomly selected to relay the wireless signal. Moreover, the authors in [11] presented a RIS-based satellite-terrestrial covert relay communication system, where a passive RIS is deployed on the surface of the building to optimize the signal reflection. However, the fixed position of relay platforms limits their adaptability in dynamic environments and reduces the flexibility of the system.

2) *Uncertainty Source and Performance Metrics in Satellite-Terrestrial Covert Communications*: In the field of satellite-terrestrial covert communications, several studies have explored modeling the uncertainty for the Warden from different sources and designing the corresponding performance metrics. For example, Guo *et al.* [12] presented a full-duplex ground receiver-based architecture of the satellite-terrestrial covert communications, where the transmit antenna of the ground receiver is used to send the jamming signal to raise the uncertainty of the Warden. In [13], the authors investigated the public message as a cover to produce the received power uncertainty in satellite-terrestrial covert communications, where the covert rate is maximized by jointly optimizing the overt

message power allocation factor. Moreover, Feng *et al.* [14] proposed the passive RIS-assisted multi-satellite cooperative covert systems and utilized the active beamforming of multiple satellites and passive beamforming of RIS to achieve the communication covertness, while ensuring the maximization of the received signal power. However, these works typically focus on introducing uncertainty through additional components such as dedicated jamming devices, which overlook the inherent noise uncertainty of the environment itself. Moreover, the majority of existing works primarily center on optimizing the covert communication rate with limited consideration given to the fairness between users.

3) *Optimization Methods for Satellite-Terrestrial Covert Communications*: Existing studies on optimization methods for satellite-terrestrial covert communication systems primarily relied on convex optimization theory. For example, Hui *et al.* [15] proposed a two-stage iterative method with the block coordinate descent to maximize the average detection error probability (DEP). In [16], the authors utilized convex optimization to minimize the average age-of-information by taking the derivative of the transmission power of the transmitter in satellite-terrestrial covert communications. Moreover, Jia *et al.* [9] maximized the minimum covert rate by using the fractional programming, semidefinite relaxation and the S-procedure. However, these methods often assume static environments or require the channel state information (CSI) of the Warden. These assumptions limit the practicality of these methods in satellite-terrestrial covert communication systems, where the instantaneous CSI of the Warden is difficult to obtain and the detection threshold of the Warden may evolve over time.

### B. Motivations and Contributions

As discussed above, existing satellite-terrestrial covert communication systems still face significant challenges in terms of the system design and optimization. To overcome these challenges, the new solution can be designed with three critical considerations. *From the perspective of the system architecture*, a flexible relay system is needed that enhances both the degree of freedom and possesses the capability of amplifying signals to improve the transmission rate of the system. *From the perspective of uncertainty sources and performance metrics*, the fairness among users must be incorporated to ensure that all users experience equitable performance while maintaining covertness without introducing extra components. *From the perspective of the optimization methods*, an efficient optimization method should be able to adapt to dynamic environments online without relying on excessive prior knowledge, thereby enabling effective decision-making even under uncertain environment conditions.

Accordingly, this paper explores an AASTAR-RIS-assisted satellite-terrestrial covert communications and presents a generative deep reinforcement learning (DRL) algorithm to optimize the sum of the fair channel capacity for all ground users in dynamic environments. A comparative analyses with related works are summarized in Table I, and the main contributions of this paper are listed as follows:

- *AASTAR-RIS-assisted Satellite-Terrestrial Covert Communication Systems*: We propose a novel AASTAR-RIS-

TABLE I  
COMPARISON BETWEEN OUR WORK AND EXISTING WORKS

Reference (2022-2025)	Satellite-Terrestrial Covert Communications			Uncertainty Sources	Performance Metrics		Decision Variables		Optimization Methods	
	Relay Mode	RIS-assisted Relay Mode	Movable RIS-assisted Relay Mode	Environmental Noise	Channel Capacity	Fairness	Trajectory	Active Beamforming	DRL	Generative Models
[8]	×	×	×	×	✓	×	×	×	×	×
[9]	×	×	×	×	✓	✓	×	✓	×	×
[10]	✓	×	×	×	×	×	×	×	×	×
[11]	✓	✓	×	×	✓	✓	×	×	×	×
[12]	×	×	×	×	✓	×	×	×	×	×
[13]	×	×	×	×	✓	×	×	×	×	×
[14]	✓	✓	×	×	✓	×	×	✓	×	×
[15]	✓	×	×	×	×	×	×	×	×	×
[16]	×	×	×	×	×	×	×	×	×	×
Our Work	✓	✓	✓	✓	✓	✓	✓	✓	✓	✓

assisted satellite-terrestrial covert communication system that leverages an LAP equipped with active STAR-RIS to act as a relay between a geosynchronous Earth orbit (GEO) satellite and the ground users. This is particularly beneficial in dense urban scenarios where the direct link is limited. Specifically, the system utilizes the flexibility of the LAP and the reconfigurable capability of an active STAR-RIS to dynamically adjust wireless channel properties, thereby enhancing the transmission rate by the signal amplification and concentration while ensuring the covert transmission by manipulating the electromagnetic wave propagation.

- *Covert Requirement Derivation and Optimization Problem Formulation:* Under the worst-case condition that the Warden has the perfect CSI information, we derive the covert requirement of the considered system based on the uncertainty of environmental noise. To further enhance the transmission rate and ensure the fairness among the ground users in such cases, we formulate an AASTAR-RIS-assisted satellite-terrestrial covert communication optimization problem (ASCCOP) by jointly optimizing the trajectory and active beamforming of the AASTAR-RIS. Notably, the formulated ASCCOP is proven as a non-convex long-term optimization problem.
- *Generative DRL Algorithm Design:* Since the formulated ASCCOP is a dynamic long-term optimization problem and involves the strict covert constraint, we propose a generative deterministic policy gradient (GDPG) algorithm to efficiently explore the decision space. Specifically, the proposed GDPG algorithm integrates the generative diffusion model (GDM) into the deterministic policy gradient (DPG) algorithm as the multimodal policy representation in the complex and high-dimensional state-action spaces, thereby generating diverse and high-quality samples through a series of denoising steps to explore the state-action space more efficiently. Moreover, we incorporate an action gradient mechanism to guide the policy towards the higher-value regions by refining better state-action pairs with the gradient ascent method.
- *Performance Validation:* Simulation results demonstrate that the proposed approach outperforms important benchmarks in terms of the sum channel capacity of all ground users, fairness among all ground users, and covertness of the system. Moreover, some deployment experiments

verify that the inference time of the proposed algorithm is in the order of tens of milliseconds, which reveals the applicability of the proposed approach.

### C. Organization and Notations

The remainder of this paper is organized as follows. We first describe the system model in Section II. In Section III, the covert requirement of the system is derived and ASCCOP is formulated and analyzed. Next, we present a generative DRL algorithm to solve the proposed ASCCOP in Section IV. Section V shows numerical results and provides corresponding discussions. Finally, Section VI concludes this paper.

*Notations:* We use plain, boldface lowercase, boldface uppercase, and calligraphic symbols to represent scalars, vectors, matrices, and sets (e.g.,  $a$ ,  $\mathbf{a}$ ,  $\mathbf{A}$ , and  $\mathcal{A}$ ), respectively. For a vector or matrix, the Euclidean and Frobenius norm are represented as  $\|\cdot\|$  and the transpose and conjugate transpose are denoted as  $\{\cdot\}^T$  and  $\{\cdot\}^H$ , respectively.  $\text{diag}(\mathbf{a})$  defines a diagonal matrix whose diagonal elements originate from  $\mathbf{a}$ . We denote the absolute value of a complex variable by  $|\cdot|$ , the Kronecker product by  $\otimes$ , and the identity matrix by  $\mathbf{I}$ . In addition, we denote the real-value and circularly symmetric complex Gaussian distribution with mean  $\boldsymbol{\mu}$  and covariance matrix  $\boldsymbol{\Lambda}$  by  $\mathcal{CN}(\boldsymbol{\mu}, \boldsymbol{\Lambda})$  and  $\mathcal{N}(\boldsymbol{\mu}, \boldsymbol{\Lambda})$ , respectively. In addition,  $\Pr(\cdot)$  represents the probability of an event, and  $\mathbb{E}[\cdot]$  denotes the expected value of a random variable.

## II. SYSTEM MODEL

In this section, we first describe the considered satellite-terrestrial communication scenario. Then, the AASTAR-RIS, channel, and communication models are given in detail. Finally, the binary hypothesis testing at the Warden is presented.

### A. Scenario Description

As shown in Fig. 1, we consider that a covert satellite-terrestrial downlink communication system, where a GEO satellite  $a$  intends to communicate covertly with multiple ground users  $\mathcal{K} \triangleq \{1, \dots, K\}$  against a passive ground Warden  $w$ . Due to the long distance and dense urban obstructions, we assume that the direct communication links between the GEO satellite and ground users are hindered by the low-gain receiving antennas and high propagation loss.

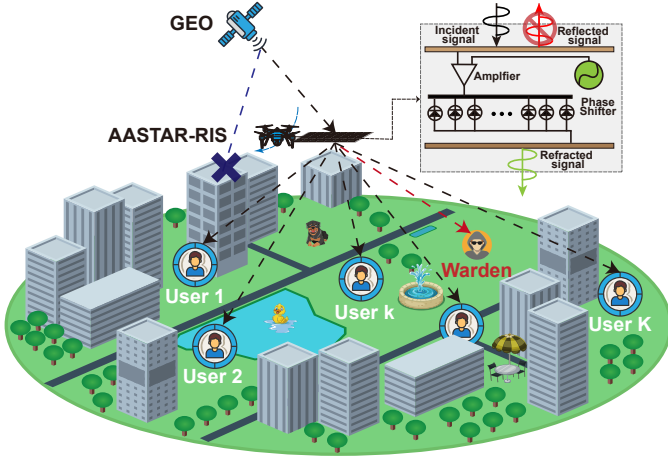


Fig. 1. An illustration of the covert satellite-terrestrial downlink communication system, where an AASTAR-RIS acts as a relay, thereby enabling signal amplification and reconfiguration to forward covert information from the GEO satellite to multiple ground users without detection by a Warden.

To overcome this, the AASTAR-RIS<sup>1</sup>  $r$  is deployed with  $M = M_x \times M_y$  transmission and reflection elements, denoted by set  $\mathcal{M} \triangleq \{1, \dots, M\}$ , to enhance covert communication between the GEO satellite and ground users<sup>2</sup>.

Without loss of generality, three-dimensional Cartesian coordinates are adopted to denote the positions of all pertinent communication nodes. In our considered scenario, all of the GEO satellite, ground users, and Warden are assumed to be stationary, with their coordinates denoted as  $\mathbf{q}_a = [x_a, y_a, z_a]^T$ ,  $\mathbf{q}_k = [x_k, y_k, 0]^T$ , and  $\mathbf{q}_w = [x_w, y_w, z_w]^T$ , respectively. Moreover, the total communication period  $T$  is divided into  $N$  time slots with an equal separation of  $\delta_t = T/N$  and each time index is denoted as  $n \in \mathcal{N} \triangleq \{1, \dots, N\}$ . At time slot  $n$ , the position of the AASTAR-RIS is denoted as  $\mathbf{q}_r[n] = [x_r[n], y_r[n], H]^T$  with the fixed altitude  $H$  to avoid collisions [7]. To facilitate analysis and optimization,  $\delta_t$  is chosen to be sufficiently small, thereby ensuring that the network environment remains quasi-static within each time slot.

In what follows, we introduce the AASTAR-RIS model, channel model and communication model to characterize the dynamics of the considered system and describe the relationship between the performance metrics and decision variables.

### B. AASTAR-RIS Model

Due to the horizontal mounting configuration of the STAR-RIS, all elements of AASTAR-RIS are set in the full transmission mode. In this mode, the transmission coefficient matrix of the AASTAR-RIS at time slot  $n$  can be given as follows [18]:

$$\Phi[n] = \text{diag}\left(\left[\beta_1[n]e^{j\phi_1[n]}, \dots, \beta_M[n]e^{j\phi_M[n]}\right]\right), \quad (1)$$

<sup>1</sup>The AASTAR-RIS can be horizontally mounted on various low aerial platforms, such as UAVs, electric vertical take-off and landing (eVTOL) aircraft or aerial vehicles, following the manner described in Ref. [17].

<sup>2</sup>In some emergency scenarios, GEO satellites can offer robust and continuous communication coverage, making them a broadly applicable solution. Our future work will consider incorporating LEO satellites, which may be suited to certain specific scenarios.

where  $\beta_m[n]$  and  $\phi_m[n]$  are the amplification gain and phase shift of the  $m$ -th element for the transmission space at time slot  $n$ , respectively.

To further enhance the transmission rate and fairness of the considered system, the AASTAR-RIS is designed to dynamically adjust its trajectory. Specifically, the position of the AASTAR-RIS at time slot  $n$  can be calculated as follows:

$$\mathbf{q}_r[n] = \mathbf{q}_r[n-1] + \mathbf{v}_r[n-1] \cdot \delta_t, \quad (2)$$

where  $\mathbf{v}_r[n-1] = [v_x[n-1], v_y[n-1], 0]^T$  is the velocity of the AASTAR-RIS at time slot  $n$ .

### C. Channel Model

Let  $\mathbf{h}_{ar}[n]$  and  $\mathbf{h}_{rk}[n]$  stand for the channel gains from the GEO satellite to the AASTAR-RIS, from the AASTAR-RIS to the ground user  $k$  and from the AASTAR-RIS to the Warden at time slot  $n$ , respectively. In this work, we consider that the channels from the GEO satellite to the AASTAR-RIS and from the AASTAR-RIS to the ground user  $k$  and the Warden are Rician fading channels [19], which can be formulated at time slot  $n$  as follows [20]:

$$\begin{aligned} \mathbf{h}_\ell[n] = & \sqrt{L_0(d_\ell[n])^{-\alpha_\ell}} \left( \sqrt{\frac{\kappa_\ell}{\kappa_\ell + 1}} \mathbf{h}_\ell^{\text{LoS}}[n] \right. \\ & \left. + \sqrt{\frac{1}{\kappa_\ell + 1}} \mathbf{h}_\ell^{\text{NLoS}}[n] \right), \ell \in \{ar, rk, rw\}, \end{aligned} \quad (3)$$

where  $L_0$  represents the path loss at the reference distance of 1 m,  $d_\ell[n]$  refers to the distance between the transmitter and receiver at time slot  $n$ , and  $\kappa_\ell$  is the Rician factor. Moreover,  $\mathbf{h}_\ell^{\text{LoS}}[n]$  and  $\mathbf{h}_\ell^{\text{NLoS}}[n]$  are the LoS and the non-LoS (NLoS) components of the link  $\ell$ , respectively. Specifically, the NLoS component can be modeled as the complex Gaussian distribution, i.e.,  $\mathbf{h}_\ell^{\text{NLoS}}[n] \sim \mathcal{CN}(\mathbf{0}, \mathbf{I})$ . For the communication link from the GEO satellite to the AASTAR-RIS, the LoS component at time slot  $n$  can be expressed as follows [21]:

$$\begin{aligned} \mathbf{h}_{ar}^{\text{LoS}}[n] = & \left[ 1, \dots, e^{-j\frac{2\pi}{\lambda} \tilde{d}_x (M_x - 1) \sin \varphi_{ar}[n] \cos \phi_{ar}[n]} \right]^T \\ & \otimes \left[ 1, \dots, e^{-j\frac{2\pi}{\lambda} \tilde{d}_y (M_y - 1) \sin \varphi_{ar}[n] \sin \phi_{ar}[n]} \right]^T, \end{aligned} \quad (4)$$

where  $\tilde{d}_x$  and  $\tilde{d}_y$  represent the antenna spacing along the  $x$ -dimension and  $y$ -dimension, respectively. Moreover,  $\sin \varphi_{ar}[n] \cos \phi_{ar}[n]$  and  $\sin \varphi_{ar}[n] \sin \phi_{ar}[n]$  are the spatial frequency along the  $x$ -dimension and  $y$ -dimension corresponding to the angle of arrival  $\varphi_{ar}[n]$  and  $\phi_{ar}[n]$ , respectively. Furthermore,  $\sin \varphi_{ar}[n] \cos \phi_{ar}[n]$  and  $\sin \varphi_{ar}[n] \sin \phi_{ar}[n]$  can be directly calculated by  $(x_r[n] - x_a) / \|\mathbf{q}_r[n] - \mathbf{q}_a\|$  and  $(y_r[n] - y_a) / \|\mathbf{q}_r[n] - \mathbf{q}_a\|$ , respectively.

Similarly, the LoS component of the communication link from the AASTAR-RIS to the ground user  $k$  and the Warden at time slot  $n$  can be respectively expressed as follows:

$$\begin{aligned} \mathbf{h}_\ell^{\text{LoS}}[n] = & \left[ 1, \dots, e^{-j\frac{2\pi}{\lambda} \tilde{d}_x (M_x - 1) \sin \varphi_\ell[n] \cos \phi_\ell[n]} \right]^T \\ & \otimes \left[ 1, \dots, e^{-j\frac{2\pi}{\lambda} \tilde{d}_y (M_y - 1) \sin \varphi_\ell[n] \sin \phi_\ell[n]} \right]^T, \ell \in \{rk, rw\}, \end{aligned} \quad (5)$$

where  $\sin \varphi_\ell[n] \cos \phi_\ell[n]$  and  $\sin \varphi_\ell[n] \sin \phi_\ell[n]$  are the spatial frequency along the  $x$ -dimension and  $y$ -dimension corresponding to the angle of departure  $\varphi_\ell[n]$  and  $\phi_\ell[n]$ , respectively.

#### D. Communication Model

In the AASTAR-RIS-assisted satellite-terrestrial downlink communication system, the received signal at the ground user  $k$  for the  $i$ -th channel at time slot  $n$  can be represented as follows:

$$\mathbf{y}_k^i[n] = \mathbf{h}_{rk}^H[n] \Phi[n] (\sqrt{p_a g_a} \mathbf{h}_{ar}[n] \mathbf{s}^i[n] + \mathbf{z}_r[n]) + z_k^i[n], \quad (6)$$

where  $p_a$  and  $g_a$  represent the transmit power and transmit gain of the GEO satellite. Moreover,  $z_k^i[n] \sim \mathcal{CN}(0, \sigma_k^2)$  denotes the additive white Gaussian noise (AWGN) at the ground user  $k$ , and  $\mathbf{z}_r[n] \sim \mathcal{CN}(\mathbf{0}, \sigma_r^2 \mathbf{I})$  represents the AWGN introduced by the power amplifier at the AASTAR-RIS.

Furthermore, the channel capacity between the GEO satellite and ground user  $k$  at time slot  $n$  can be expressed as follows:

$$r_{ak}[n] = \log_2 \left( 1 + \frac{p_a g_a \left| \mathbf{h}_{rk}^H[n] \Phi[n] \mathbf{h}_{ar}[n] \right|^2}{\sigma_r^2 \left\| \mathbf{h}_{rk}^H[n] \Phi[n] \right\|^2 + \sigma_k^2} \right). \quad (7)$$

#### E. Binary Hypothesis Testing at Warden

Let the null hypothesis  $\mathcal{H}_0$  and alternative hypothesis  $\mathcal{H}_1$  denote the two circumstances that the GEO satellite is silent and sends the covert message to ground users, respectively. In particular, the Warden determines whether the GEO satellite is transmitting on the basis of the power of the signal received by a radiometer [6]. For the  $i$ -th channel at time slot  $n$ , the received signal at the Warden from the GEO satellite can be described as follows:

$$\mathbf{y}_w^i[n] = \begin{cases} \mathbf{h}_{rw}^H[n] \Phi[n] (\sqrt{p_a g_a} \mathbf{h}_{ar}[n] \mathbf{s}^i[n] + \mathbf{z}_r[n]) & \mathcal{H}_1, \\ + z_w^i[n], & \\ z_w^i[n], & \mathcal{H}_0, \end{cases} \quad (8)$$

where  $z_w^i[n] \sim \mathcal{CN}(0, \sigma_w^2)$  are the AWGN at the Warden.

In the binary testing problem, the decision rule of the Warden can be expressed as follows [20]:

$$T_w[n] = \frac{1}{L} \sum_{i=1}^L |y_w^i[n]|^2 \stackrel{\mathcal{D}_1}{\geq} \tau[n], \quad (9)$$

where  $L$  represents the number of signal samples of the Warden, and  $\tau[n]$  represents the decision threshold of the Warden at time slot  $n$ . Moreover,  $\mathcal{D}_0$  and  $\mathcal{D}_1$  are the decision results while supporting  $\mathcal{H}_0$  and  $\mathcal{H}_1$ , respectively. Similar to [22], we consider  $L \rightarrow \infty$ , which means that an infinite amount of samples can be used at the Warden.

As such, we can observe that optimizing the trajectory and active beamforming of the AASTAR-RIS can not only improve the channel capacity of ground users, but also reduce the risk of detection by the Warden.

### III. PROBLEM FORMULATION

In this section, we first derive the covert requirement of the considered covert communication system at each time slot. Based on this, the ASCCOP is formulated and analyzed.

#### A. Covert Requirement

The detection decision of the Warden involves two types of errors, which are the false alarm (FA) and miss detection (MD). The FA occurs when the Warden incorrectly assumes that the transmission is occurring while the GEO satellite remains silent. Conversely, the MD happens when the Warden fails to recognize that the GEO satellite is transmitting. Mathematically, the FA and MD probabilities are denoted as  $P_{\text{FA}}[n] = \Pr(\mathcal{D}_1 | \mathcal{H}_0)[n]$  and  $P_{\text{MD}}[n] = \Pr(\mathcal{D}_0 | \mathcal{H}_1)[n]$ , respectively. Therefore, the DEP can be defined as follows:

$$\begin{aligned} \xi[n] &= P_{\text{FA}}[n] + P_{\text{MD}}[n] \\ &= \Pr(\sigma_w^2 \geq \tau[n]) + \Pr(\iota[n] + \sigma_w^2 \leq \tau[n]), \end{aligned} \quad (10)$$

where  $\iota[n] = p_a g_a \left| \mathbf{h}_{rw}^H[n] \Phi[n] \mathbf{h}_{ar}[n] \right|^2 + \sigma_r^2 \left\| \mathbf{h}_{rw}^H[n] \Phi[n] \right\|^2$ .

Due to variations of the wireless communication environment, the noise uncertainty of the Warden can be described as follows [22]:

$$f_{\sigma_w^2}(x) = \begin{cases} \frac{1}{2 \ln(\rho)x} & \text{if } \frac{1}{\rho} \hat{\sigma}_w^2 \leq x \leq \rho \hat{\sigma}_w^2, \\ 0, & \text{otherwise,} \end{cases} \quad (11)$$

where  $\rho$  and  $\hat{\sigma}_w^2$  represent the noise uncertainty and nominal noise power, respectively. Considering the noise uncertainty and the scenario where the Warden has the perfect CSI, the DEP in Eq. (10) can be further formulated as follows:

$$\xi[n] = 1 - \int_{\max(\tau[n] - \iota[n], \frac{\hat{\sigma}_w^2}{\rho})}^{\tau[n]} \frac{1}{2 \ln(\rho)x} dx. \quad (12)$$

Then, the derivative of  $\xi[n]$  with respect to  $\tau[n]$  can be calculated as follows:

$$\frac{\partial \xi[n]}{\partial \tau[n]} = \begin{cases} -\frac{1}{(2 \ln \rho) \tau[n]}, & \tau[n] \leq \iota[n] + \frac{\hat{\sigma}_w^2}{\rho}, \\ \frac{1}{2 \ln \rho} \left( \frac{1}{\tau[n] - \iota[n]} - \frac{1}{\tau[n]} \right), & \tau[n] > \iota[n] + \frac{\hat{\sigma}_w^2}{\rho}. \end{cases} \quad (13)$$

When  $\tau[n] \leq \iota[n] + \frac{\hat{\sigma}_w^2}{\rho}$ , the derivative is negative, thereby implying that  $\xi[n]$  decreases with respect to  $\tau[n]$ . When  $\tau[n] > \iota[n] + \frac{\hat{\sigma}_w^2}{\rho}$ , the derivative is positive, and thus  $\xi[n]$  increases with respect to  $\tau[n]$ . Moreover, the optimal detection threshold should be within  $[\frac{\hat{\sigma}_w^2}{\rho}, \rho \hat{\sigma}_w^2]$ . Therefore, the optimal detection threshold for the Warden at time slot  $n$  can be calculated as follows:

$$\tau^*[n] = \min \left( \iota[n] + \frac{\hat{\sigma}_w^2}{\rho}, \rho \hat{\sigma}_w^2 \right). \quad (14)$$

Substituting  $\tau^*[n]$  into Eq. (12), the minimal DEP can be calculated as follows:

$$\xi^*[n] = \begin{cases} 1 - \frac{1}{(2 \ln \rho)x} \ln \left( 1 + \frac{\rho \iota[n]}{\hat{\sigma}_w^2} \right), & \text{if } \iota[n] \leq \rho \hat{\sigma}_w^2 - \frac{\hat{\sigma}_w^2}{\rho}, \\ 0, & \text{otherwise.} \end{cases} \quad (15)$$

The AASTAR-RIS-assisted satellite-terrestrial covert communication system aims to ensure that  $\xi^*[n] \geq 1 - \varepsilon$ , where  $\varepsilon$  is a small constant to control the covert requirement. Combining Eq. (15), the considered system covert requirement at time slot  $n$  can be reformulated as follows:

$$\iota[n] < \min \left( \rho \hat{\sigma}_w^2 - \frac{\hat{\sigma}_w^2}{\rho}, \frac{(\rho^{2\varepsilon} - 1) \hat{\sigma}_w^2}{\rho} \right). \quad (16)$$

## B. Problem Formulation

As outlined earlier, we define the fairness index of the channel capacity according to Jain's index to guarantee the fairness among all ground users, which can be represented as follows [23]:

$$J[n] = \frac{\left(\sum_{k=1}^K r_{ak}[n]\right)^2}{K \left(\sum_{k=1}^K r_{ak}[n]^2\right)}. \quad (17)$$

We aim to maximize the sum of the fair channel capacity for all ground users under the worst situation subject to the covert constraint via a joint design of the trajectory and active beamforming of the AASTAR-RIS. Defining  $\mathbf{v}_r \triangleq \{\mathbf{v}_r[n], \forall n\}$ ,  $\beta \triangleq \{\beta_m[n], \forall m, n\}$  and  $\phi \triangleq \{\phi_m[n], \forall m, n\}$ , the ASCCOP can be formulated as follows:

$$\max_{\{\mathbf{v}_r, \beta, \phi\}} \sum_{n=1}^N J[n] \sum_{k=1}^K r_{ak}[n] \quad (18a)$$

$$\text{s.t.} \quad (16), \quad (18b)$$

$$\|\mathbf{q}_r[n+1] - \mathbf{q}_r[n]\| \leq v_{\max} \cdot \delta_t, \quad \forall n \in \mathcal{N}, \quad (18c)$$

$$\beta_m[n] > 1, \quad \forall m \in \mathcal{M}, n \in \mathcal{N}, \quad (18d)$$

$$\phi_m[n] \in [0, 2\pi], \quad \forall m \in \mathcal{M}, n \in \mathcal{N}, \quad (18e)$$

$$\|\Phi[n] \mathbf{h}_{ar}[n]\|^2 + \sigma_r^2 \|\Phi[n]\|^2 < P_{\max}^{\text{active}}, \quad \forall n \in \mathcal{N}, \quad (18f)$$

$$X_{\min} \leq x_r[n] \leq X_{\max}, \quad \forall n \in \mathcal{N}, \quad (18g)$$

$$Y_{\min} \leq y_r[n] \leq Y_{\max}, \quad \forall n \in \mathcal{N}, \quad (18h)$$

where the constraints (18c), (18d) and (18e) confine the velocity, amplification gains and phase shifts of the AASTAR-RIS, respectively. Moreover, the constraint (18f) is to ensure that the transmit power budget of the AASTAR-RIS fails to exceed the maximum restriction. In addition, the constraints (18g) and (18h) represent the boundary constraints for the AASTAR-RIS.

Note that the specific challenges associated with the formulated ASCCOP are listed as follows.

- *Non-convexity and Long-term Optimization:* The ASCCOP is inherently non-convex since the optimization objective is non-convex with respect to  $\mathbf{v}_r$ ,  $\beta$  and  $\phi$ , and the feasible solution space is also not a convex set due to the existence of constraints (16) and (18f). Moreover, since the goal is to maximize the fair channel capacity over a long-term horizon, the optimization requires taking into account future states of the system.
- *Dynamic Environment and Imperfect Information:* The environment in which the AASTAR-RIS operates is highly dynamic with fluctuating channel conditions. Moreover, another significant challenge arises from the lack of real-time CSI about the Warden.

Conventional methods typically struggle with this because they require knowledge of future states, which are often uncertain and not directly observable in real-time. In this case, DRL has shown promise in addressing dynamic and uncertain environments in wireless communications [24], [25]. Therefore, we transform the ASCCOP in the context of DRL and design an effective DRL-based algorithm to solve it.

## IV. PROPOSED ALGORITHM

In this section, we first reformulate the considered ASCCOP as a Markov decision process. Then, we introduce the basics of the conventional DPG algorithm. Next, we design the GDPG algorithm to solve the proposed ASCCOP. Finally, we analyze the complexity of the proposed GDPG algorithm.

### A. MDP Formulation

The dynamic decision process in the proposed ASCCOP can be naturally modeled as an MDP, which can be described as a 5-tuple  $\Omega = \langle \mathcal{S}, \mathcal{A}, R, P, \gamma \rangle$  [26]. At each time slot  $n$ , the agent receives the state  $\mathbf{s}[n]$  from the environment and selects an action  $\mathbf{a}[n] \in \mathcal{A}$  based on its policy  $\pi(\mathbf{a}|\mathbf{s})$ . Then, the next state is generated based on the transition probability  $P(\mathbf{s}'|\mathbf{s}, \mathbf{a})$ , and the agent receives the reward  $r[n] = R(\mathbf{s}[n], \mathbf{a}[n])$  from the environment as a feedback. Moreover,  $\gamma \in (0, 1]$  is the discount factor that balances immediate and future rewards. Accordingly, the details of each element in the considered ASCCOP are explained as follows.

1) *Action:* According to the design of ASCCOP, the action at time slot  $n$  contains the trajectory control and active beamforming of the AASTAR-RIS, which can be defined as follows:

$$\mathbf{a}[n] = \{\mathbf{v}_r[n], \beta_1[n], \dots, \beta_M[n], \phi_1[n], \dots, \phi_M[n]\}. \quad (19)$$

2) *State:* At each time slot, the state space represents the observable information relevant to the decision-making process. In the context of ASCCOP, the state space consists of the following three components:

- *Position Information:* The system considers all entities remain at a constant altitude. This information is represented through the horizontal coordinates of the AASTAR-RIS, positions of ground users, and position of the Warden.
- *Instantaneous CSI Information:* This part contains real-time CSIs between the GEO satellite and AASTAR-RIS as well as between the AASTAR-RIS and ground users. Note that the CSIs are decomposed into their real and imaginary components as the input of neural networks.
- *Historical Information:* Because the historical information can provide necessary information for making decisions in the current time slot, last action, channel capacities between the GEO satellite and all users, and the received reward are contained in this part.

Thus, the state  $\mathbf{s}[n]$  at time slot  $n$  can be written as follows:

$$\mathbf{s}[n] = \{x_r[n], y_r[n], x_1, \dots, x_K, y_1, \dots, y_K, x_w, y_w, \mathbf{h}_{ar}[n], \mathbf{h}_{r1}[n], \dots, \mathbf{h}_{rK}[n], \mathbf{a}[n-1], r_{a1}[n-1], \dots, r_{aK}[n-1], r[n-1]\}. \quad (20)$$

3) *Reward:* The optimization objective of the formulated ASCCOP aims to maximize the sum of fair channel capacity among the ground users while satisfying the system constraints. To achieve this, the reward at time slot  $n$  is defined as follows:

$$r[n] = J[n] \sum_{k=1}^K r_{ak}[n] + r_{pc} + r_{pr} + r_{pp}, \quad (21)$$

where  $r_{pc}$  is the penalty when the minimal DEP falls below the required threshold. Moreover,  $r_{pr}$  is the penalty when the AASTAR-RIS exceeds the maximum power consumption and  $r_{pp}$  is the penalty when its trajectory adjustments violate the movement or area constraints.

### B. Conventional Deterministic Policy Gradient Algorithm

The DPG algorithm is a classic reinforcement learning method that combines both policy-based and value-based methods [27], which enables simultaneous action generation and evaluation, thus improving training efficiency and decision-making in complex environments. Specifically, the main idea of the DPG algorithm primarily relies on policy evaluation and policy improvement to optimize decision-making processes. Let  $\{\mathbf{s}[n], \mathbf{a}[n], \mathbf{s}[n+1], r[n]\}_{n \geq 0} \sim \pi_\theta$  be a trajectory sampled from the parameterized policy  $\pi_\theta$ , then the DPG algorithm aims to find an optimal policy  $\pi_\theta^*$  that maximizes the expected cumulative return, which can be expressed as follows:

$$\pi_\theta^* = \arg \max_{\pi_\theta} \mathbb{E}_{\pi_\theta} \left[ \sum_{n=0}^N \gamma^n R(\mathbf{s}[n], \mathbf{a}[n]) \right]. \quad (22)$$

1) *Policy Evaluation*: The core objective of policy evaluation is to compute the state-action value function  $Q_\phi^{\pi_\theta}(\mathbf{s}, \mathbf{a})$  for a given policy  $\pi_\theta$  in an environment. This function represents the expected cumulative return when following  $\pi_\theta$ , starting from state  $\mathbf{s}$  and taking action  $\mathbf{a}$ . Specifically, the Bellman equation of  $Q_\phi^{\pi_\theta}(\mathbf{s}, \mathbf{a})$  is given by:

$$Q_\phi^{\pi_\theta}(\mathbf{s}, \mathbf{a}) = \mathbb{E}_{\mathbf{s}' \sim P(\mathbf{s}'|\mathbf{s}, \mathbf{a})} \left[ R(\mathbf{s}, \mathbf{a}) + \gamma \mathbb{E}_{\mathbf{a}' \sim \pi_\theta} Q_\phi^{\pi_\theta}(\mathbf{s}', \mathbf{a}') \right]. \quad (23)$$

To minimize the difference between the estimated action-value function and the Bellman target, the loss function is defined as follows:

$$\mathcal{L}(\phi) = \mathbb{E} \left[ \left| Q_\phi^{\pi_\theta}(\mathbf{s}, \mathbf{a}) - \left( R(\mathbf{s}, \mathbf{a}) + \gamma \mathbb{E}_{\mathbf{a}' \sim \pi_\theta} Q_\phi^{\pi_\theta}(\mathbf{s}', \mathbf{a}') \right) \right|^2 \right]. \quad (24)$$

2) *Policy Improvement*: The policy gradient theorem provides a foundation for policy improvement and this process can be expressed as follows [27]:

$$\nabla_\theta J(\pi_\theta) = \mathbb{E}_{(\mathbf{s}, \mathbf{a}) \sim \pi_\theta} \left[ \nabla_\theta \log \pi_\theta(\mathbf{a}|\mathbf{s}) Q_\phi^{\pi_\theta}(\mathbf{s}, \mathbf{a}) \right]. \quad (25)$$

By iterating between policy evaluation and policy improvement, the DPG algorithm can converge to an optimal policy  $\pi_\theta^*$ .

### C. Generative Deterministic Policy Gradient Algorithm

1) *GDM for Policy Representation*: When addressing the proposed ASCOP, the conventional DPG algorithm faces two primary challenges. First, this method inherently struggles to explore the complex, high-dimensional and multimodal state-action spaces due to its reliance on unimodal Gaussian distribution [28]. Second, the frequent penalties imposed by covert constraints further exacerbate this issue by discouraging the agent from effectively leveraging the rare positive reinforcement signals.

Compared to fully-connected deep neural networks adopted in the conventional DPG algorithm, GDM provides certain distinct advantages. Specifically, GDM excels in generating the diverse and high-quality samples, which is particularly beneficial for exploring the vast and complex state-action spaces [29]. Moreover, the superior feature representation capability of GDM enables a deeper understanding of the environmental state, which is crucial for effective decision-making in complex scenarios.

According to [29], the basic process of GDM includes the forward process and reverse process. Specifically, the forward process of GDM incrementally corrupts a data sample by adding Gaussian noise over a series of time steps, thereby transforming its distribution into one that approximates pure Gaussian noise. More formally, this forward procedure constitutes a Markov chain, which can be defined as follows:

$$q(\mathbf{x}_{1:T}|\mathbf{x}_0) = \sum_{t=1}^T q(\mathbf{x}_t|\mathbf{x}_{t-1}), \quad (26)$$

where  $T$  is the total number of diffusion steps, and  $q(\mathbf{x}_t|\mathbf{x}_{t-1}) = \mathcal{N}(\mathbf{x}_t; \sqrt{1 - \nu_t} \mathbf{x}_{t-1}, \nu_t \mathbf{I})$  represents the transition kernel of the forward process. Moreover,  $\nu_t \in (0, 1)$  is a diffusion weight to control the speed of diffusion. After applying a series of derivations, the joint transition over all time steps can be marginalized to yield a closed-form expression for the distribution of  $\mathbf{x}_t$  conditioned on  $\mathbf{x}_0$ , which can be computed as follows [30]:

$$q(\mathbf{x}_t|\mathbf{x}_0) = \mathcal{N}\left(\sqrt{\bar{\alpha}_t} \mathbf{x}_0, (1 - \bar{\alpha}_t) \mathbf{I}\right), \quad (27)$$

where  $\bar{\alpha}_t = \prod_{i=1}^t (1 - \nu_i)$ . Given the closed-form expression, we can sample any  $\mathbf{x}_t$  without iterating through the entire Markov chain.

The reverse process in GDM is to recover the original data distribution from a noise-corrupted sample by progressively removing the added noise at each time step. Specifically, the reverse process begins by initializing the latent variable at time step  $T$  with  $\mathbf{x}_T \sim \mathcal{N}(\mathbf{0}, \mathbf{I})$ . Since the statistical distribution  $q(\mathbf{x}_{t-1}|\mathbf{x}_t)$  is intractable, a parameterized model is used to estimate this distribution, which can be expressed as follows:

$$p_\theta(\mathbf{x}_{t-1}|\mathbf{x}_t) = \mathcal{N}(\mu_\theta(\mathbf{x}_t, t), \Sigma_\theta(\mathbf{x}_t, t)), \quad (28)$$

where  $\mu_\theta(\mathbf{x}_t, t)$  and  $\Sigma_\theta(\mathbf{x}_t, t)$  represent the mean and the covariance matrix of the predicting noise at time step  $t$ , respectively. To incorporate specific semantic attributes into the reverse process, the conditional GDM can provide additional information to guide each denoising step [31]. Specifically, the reverse transition chain can be further expressed as follows:

$$q(\mathbf{x}_{t-1}|\mathbf{x}_t, \mathbf{g}) = \mathcal{N}\left(\frac{1}{\sqrt{1 - \nu_t}} \left( \mathbf{x}_t - \frac{\nu_t}{\sqrt{1 - \bar{\alpha}_t}} \epsilon_\theta(\mathbf{x}_t, \mathbf{g}, t) \right), \nu_t \mathbf{I}\right), \quad (29)$$

where  $\mathbf{g}$  is the condition information of reverse process. Furthermore, the parametrized noise-prediction network  $\epsilon_\theta(\mathbf{x}_t, \mathbf{g}, t)$  is used to estimate the noise component of the current data  $\mathbf{x}_t$  at each subsequent time step  $t$ . Moreover, a weighted version of the evidence lower bound (ELBO) can be adopted to learn  $\epsilon_\theta(\mathbf{x}_t, \mathbf{g}, t)$ , which can be written as follows:

$$\mathcal{L}(\theta) = \mathbb{E} \left[ \left| \epsilon - \epsilon_\theta(\sqrt{\bar{\alpha}_t} \mathbf{x}_0 + \sqrt{1 - \bar{\alpha}_t} \mathbf{z}, \mathbf{g}, t) \right|^2 \right], \quad (30)$$

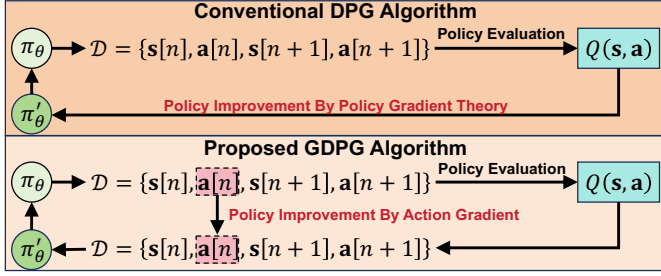


Fig. 2. Comparison of the policy improvement between the conventional DPG algorithm and the proposed GDBG algorithm.

---

### Algorithm 1: Policy Representation Based on GDM

---

**Input:**  $T, \epsilon_\theta(\cdot), s[n]$

**Output:**  $a[n]$

- 1 Initialize  $\mathbf{x}_T \sim \mathcal{N}(\mathbf{0}, \mathbf{I})$ ;
  - 2 **for**  $t \leftarrow T$  **to** 1 **do**
  - 3      $\hat{\epsilon} \leftarrow \epsilon_\theta(\mathbf{x}_t, s[n], t)$ ;
  - 4      $\mathbf{z} \sim \mathcal{N}(\mathbf{0}, \mathbf{I})$  if  $t > 1$  else  $\mathbf{z} = \mathbf{0}$ ;
  - 5      $\mathbf{x}_{t-1} \leftarrow \frac{1}{\sqrt{1-\nu_t}} \left( \mathbf{x}_t - \frac{\nu_t}{\sqrt{1-\alpha_t}} \hat{\epsilon} \right) + \sqrt{\nu_t} \mathbf{z}$ ;
  - 6 **return**  $a[n] \leftarrow \mathbf{x}_0$ ;
- 

where  $\epsilon$  is a random sample from  $\mathcal{N}(\mathbf{0}, \mathbf{I})$ . To introduce the GDM as the policy representation into the DPG algorithm, we regard the reverse diffusion process as a generative mechanism that produces actions conditioned on the current state, which is illustrated in the Algorithm 1.

2) *Action Gradient for Policy Improvement:* As shown in Eq. (30), GDM merely learns to approximate the distribution of training samples produced by the current policy  $\pi_\theta$ . As such, it does not intrinsically offer a mechanism to optimize the policy beyond the scope of the data on which it is trained. Different from the conventional DPG algorithm, direct policy improvement through the policy gradient theorem is not feasible in this setting, as the diffusion-based policy is not parameterized straightforwardly but is instead learned via a stochastic process. Therefore, we adopt an action gradient mechanism to enable policy improvement, which is shown in Fig. 2. Specifically, a given state-action pair  $(s, \mathbf{a})$  can be converted into a better state-action pair by the gradient ascent method, which can be represented as follows [30]:

$$\mathbf{a} = \mathbf{a} + \eta_a \mathbb{E}_{(s, \mathbf{a}) \in \mathcal{D}} [\nabla_{\mathbf{a}} Q_{\phi}^{\pi_\theta}(s, \mathbf{a})] \quad (31)$$

where  $\eta_a$  is the step-size, and  $\mathcal{D}$  represents the replay buffer used to store the experiences of the agent in the environment. Moreover,  $\nabla_{\mathbf{a}} Q_{\phi}^{\pi_\theta}(s, \mathbf{a})$  is referred to as the action gradient. By replacing the original state-action pair with the improved pair, the GDM-based policy can be updated continually, ensuring  $\pi_\theta^{new} \succeq \pi_\theta$  and thereby accomplishing policy improvement.

#### D. Overall Structure and Complexity Analysis

Similar to approaches used in [32], [33], we employ a target GDM network  $\pi_{t\theta}$ , and a double critic networks  $Q_{\phi_1}$

---

### Algorithm 2: GDBG Algorithm Training Procedure

---

- 1 Initialize GDM network parameters  $\theta$ , critic network parameters  $\phi_1$  and  $\phi_2$  as well as their corresponding target network parameters  $t\theta, t\phi_1$  and  $t\phi_2$ ;
  - 2 Initialize replay buffer  $\mathcal{D}$ ;
  - 3 **for each episode do**
  - 4     Reset environment and initialize state  $s[0]$ ;
  - 5     **for each time step  $n$  do**
  - 6         Select action  $\mathbf{a}[n]$  by **Algorithm 1**;
  - 7         Execute action  $\mathbf{a}[n]$ , observe reward  $r[n]$  and next state  $s[n+1]$ ;
  - 8         Store transition  $(s[n], \mathbf{a}[n], r[n], s[n+1])$  in replay buffer  $\mathcal{D}$ ;
  - 9         **if**  $current\_step \geq start\_learning\_step$  **then**
  - 10             Sample a batch from  $\mathcal{D}$ ;
  - 11             Compute the loss of critic networks by Eq. (32) and update critic networks by the gradient descent method;
  - 12             Compute action gradients  $\nabla_{\mathbf{a}} Q_{\phi}^{\pi_\theta}(s, \mathbf{a})$  and update state-action pair of batch by Eq. (31);
  - 13             Compute weighted ELBO loss by Eq. (30) and update GDM network;
  - 14             Soft update target networks by Eq. (33)
- 

and  $Q_{\phi_2}$  alongside their corresponding target critic networks  $Q_{t\phi_1}$  and  $Q_{t\phi_2}$  to avoid abrupt distribution shifts and address Q-value overestimation. Specifically, the loss function of the critic network can be expressed as follows:

$$\mathcal{L}(\phi_i) = \mathbb{E}_{(s, \mathbf{a}, r, s') \sim \mathcal{D}} \left[ |Q_{\phi_i}(s, \mathbf{a}) - y|^2 \right], \quad i \in \{1, 2\}, \quad (32)$$

where  $y = \left( r + \gamma \min_{j \in \{1, 2\}} Q_{t\phi_j}(s', \pi_{t\theta}(s')) \right)$ . Moreover, we periodically update the target networks for both the actor and the critic. Specifically, the parameters of the target networks are updated as follows:

$$\begin{aligned} t\theta &\leftarrow \tau\theta + (1 - \tau)t\theta, \\ t\phi_i &\leftarrow \tau\phi_i + (1 - \tau)t\phi_i, \quad i \in \{1, 2\}, \end{aligned} \quad (33)$$

where  $\tau$  is a small positive constant that controls the rate of the soft update.

The structure of the proposed GDBG algorithm for the ASCCOP is illustrated in Fig. 3 and the detailed implementation is outlined in Algorithm 2. Next, we analyze the computational and space complexity of the proposed GDBG algorithm for both training and execution phases. Specifically, the analysis focuses on the integration of GDM and DRL components, including diffusion-based action generation, dual-critic optimization, and action gradient mechanisms.

1) *Training Phase:* Let  $G, B, |\phi|$  and  $|\theta|$  represent the number of training episodes, batch size, the number of critic network parameters, and the number of GDM network parameters, respectively. Then, the total computational complexity during the training phase is  $\mathcal{O}(GN(B + (4 + T)|\theta| + 6|\phi|))$ .



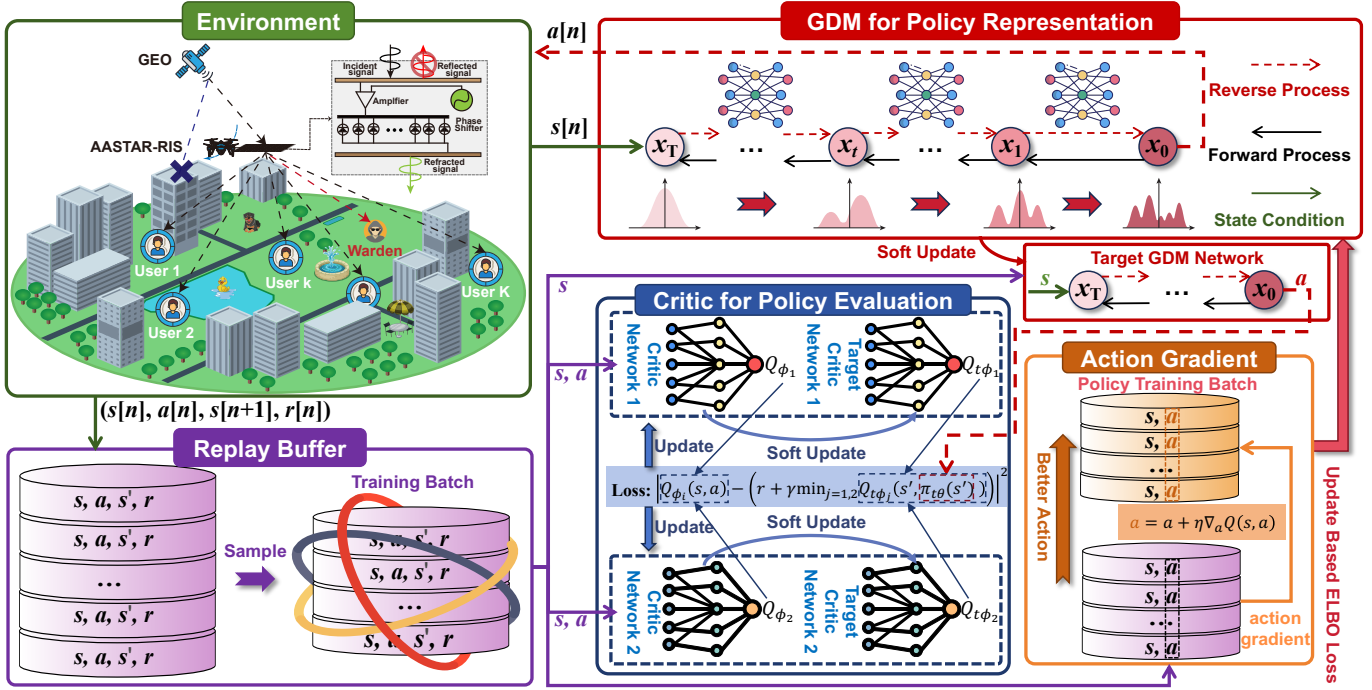


Fig. 3. The overall architecture of the proposed GDBG algorithm to solve the ASCCOP.

Specifically, the computational complexity of the training phase is summarized as follows [30]:

- *Network Initialization*: This process involves initializing two critic networks, a GDM network, and their target networks, thereby increasing the overhead  $\mathcal{O}(4|\phi|+2|\theta|)$ .
- *Action Selection*: GDM-based action generation at each step needs to perform  $T$  denoising steps, thereby introducing the overhead  $\mathcal{O}(GNT|\theta|)$  during the entire training phase.
- *Network Updates*: The overhead of the network update process includes several components. The parameter update for the two critic networks incurs the overhead  $\mathcal{O}(2GN|\phi|)$ . Moreover, action gradient improvements add the overhead  $\mathcal{O}(GNB)$ . Additionally, the GDM network update introduces the overhead  $\mathcal{O}(GNT|\theta|)$ . Finally, the soft update operation results in the overhead  $\mathcal{O}(GN|\phi|+2GN|\theta|)$ . As a result, the overall complexity is  $\mathcal{O}(GN(B+2|\theta|+4|\phi|))$ .

Let  $|s|$  and  $|a|$  represent the dimensions of state and action spaces, respectively. Then, the space complexity during training phase is  $\mathcal{O}(4|\phi|+2|\theta|+D(2|s|+|a|+1))$ , which mainly includes the storage of network parameters  $\mathcal{O}(4|\phi|+2|\theta|)$  and the replay buffer storage  $\mathcal{O}(D(2|s|+|a|+1))$ .

2) *Execution Phase*: The computational complexity during execution is  $\mathcal{O}(T|\theta|)$ , as each action decision requires  $T$  denoising steps by the GDM network. The space complexity during the execution phase is  $\mathcal{O}(|\theta|)$ , which involves only the storage of the GDM network parameters.

## V. PERFORMANCE EVALUATION

In this section, we first describe our simulation setup. Then, comprehensive results are presented to assess the effectiveness,

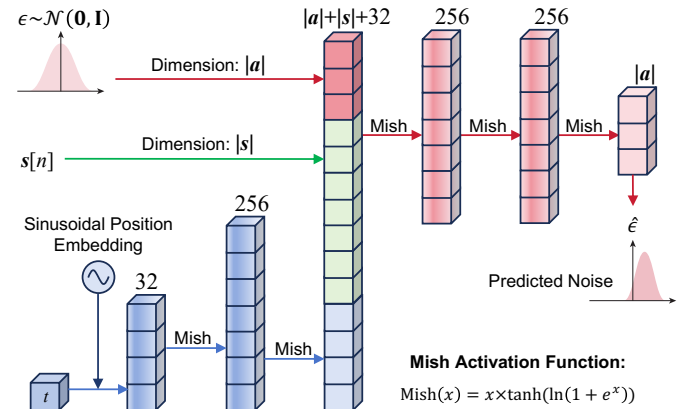


Fig. 4. Architecture of GDM network with Mish activation function [34] for non-monotonic gradient flow, and sinusoidal position embedding for efficient encoding of temporal information in the reverse process.

robustness and practicality of the proposed approach.

### A. Simulation Setup

1) *Environment and Model Details*: In this work, we consider the service area as a square region with 200 m by 200 m. In this region, 5 ground users are served by an LAP, operating at  $H = 100$  m, and equipped with a  $4 \times 4$  active STAR-RIS array to facilitate the wireless covert transmission between a GEO satellite and the ground users. For the proposed GDBG algorithm, we utilize the Adam optimizer with a learning rate  $3 \times 10^{-4}$  for both the GDM network and the critic networks, while setting  $\eta_a = 3 \times 10^{-2}$  for the action gradient. The specific GDM network structure is exhibited in Fig. 4 and

TABLE II  
SIMULATION PARAMETERS

	Parameter	Value	Parameter	Value	
Environment	$N$	50	$\delta t$	1 s	
	$\alpha_{ar}$	2.1	$\alpha_{rk}$	2.5	
	$\alpha_{rw}$	2.7	$\kappa_{ar}$	5	
	$\kappa_{kr}$	3	$\kappa_{rw}$	3	
	$v_{max}$	20 m/s	$\lambda$	0.15 m	
	$L_0$	-38 dB	$\tilde{d}_x, \tilde{d}_y$	0.075 m	
	$p_a$	59 dBW/MHz	$g_a$	51 dBi	
	$\sigma_r^2, \sigma_k^2, \sigma_w^2$	-174 dBm/Hz	$\rho$	3 dB	
	Algorithm	$\gamma$	0.95	$T$	10
		$\tau$	0.005	$B$	256
$D$		100000	$G$	20000	

other key parameters for the environment and algorithm are summarized in Table II.

2) *Benchmarks*: To evaluate the effectiveness of the proposed approach and the GDPG algorithm, we compare both the overall approach and algorithm performances against several other approaches and algorithms.

- *Random*: At each time slot, actions are randomly selected from the action space. It is used primarily as a lower-bound baseline, which indicates the worst performance of the considered system.
- *Non-active STAR-RIS (NA)*: In this approach, the STAR-RIS mounted on the LAP is passive, which does not amplify the transmission signals.
- *Only Trajectory Optimization (OTO)*: This mode focuses solely on optimizing the trajectory of the AASTAR-RIS while keeping the active beamforming of the AASTAR-RIS fixed.
- *Only Active Beamforming Optimization (OABO)*: In this case, only the active beamforming of the AASTAR-RIS is optimized, while the position of the AASTAR-RIS remains unchanged.
- *State-of-the-Art DRL Algorithms*: The deep deterministic policy gradient (DDPG) and twin delayed DDPG (TD3) are the earliest actor-critic algorithms designed for continuous action spaces [32]. Moreover, soft actor-critic (SAC) is based on the maximum entropy reinforcement learning framework and also serves as a baseline [33].

In order to make a fair performance comparison with benchmarks, the neural network architectures of all DRL-

based benchmarks comprise two hidden layers for both the actor and critic networks, with each layer containing 256 neurons. In addition, the learning rate is consistent with the proposed GDPG algorithm.

### B. Simulation Results

1) *Comparison with Other Approaches*: We compare our approach with some other approaches in terms of the communication performance and covert of the system. As shown in Fig. 5, NA approach stands out in terms of covert constraint compliance while remaining relatively low in terms of its mean sum channel capacity compared to other approaches with active STAR-RIS since the signal amplification is limited. On the other hand, our approach not only achieves higher communication performance but also maintains covert constraint compliance effectively. Unlike the approaches that only optimize certain aspects, such as OTO or OABO approaches, our approach integrates a holistic optimization strategy, thereby addressing both the communication performance and system covertness simultaneously.

2) *Comparison with State-of-the-Art DRL Algorithms*: Fig. 6(a) illustrates the reward per episode of the proposed GDPG algorithm in comparison to other state-of-the-art DRL algorithms during the training process. As can be seen, the proposed GDPG algorithm consistently outperforms the other algorithms with a steady increase in reward over the training time. The success of the GDPG algorithm lies in the use of the GDM, which improves the exploration and policy optimization by generating the diverse and high-quality samples through its denoising process, thereby resulting in higher overall rewards, especially in the complex satellite-terrestrial covert communication scenarios. Moreover, DDPG and TD3 demonstrate initial improvements in rewards during the early stages of training, but their progress slows and eventually plateaus. This indicates that although they achieve early gains, their performance is constrained by limited exploration, thereby leading to suboptimal policy. Finally, SAC performs better than DDPG and TD3 with a more consistent increase in rewards. However, it still has lower performance than that of the GDPG algorithm, thereby illustrating that SAC lacks the same level of exploration efficiency and optimization capabilities provided by the proposed GDPG algorithm.

Fig. 6(b) shows the mean sum channel capacity per step of the proposed GDPG algorithm in comparison to other state-of-the-art DRL algorithms. The performance achieved by the proposed GDPG algorithm is notably higher than that of other algorithms. This indicates that the GDM-enabled DRL algorithm is more effective in leveraging its representation and exploration capabilities in the large state and action spaces. Another important metric is the fairness index, which is presented in Fig. 6(c). As can be seen, the GDPG algorithm maintains the highest fairness index across all algorithms. While SAC converges faster and experiences greater fluctuations in terms of the fairness index when compared to other algorithms, the GDPG algorithm achieves the fastest convergence and consistently maintains a higher fairness index, owing to its denoising process and more effective exploration of the action space.

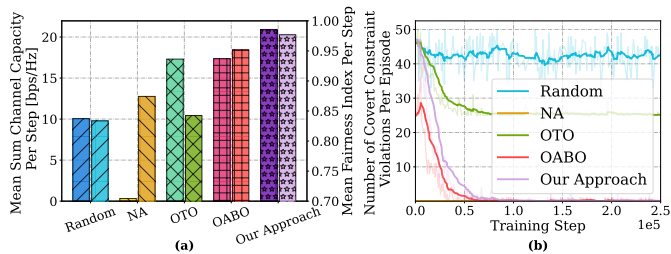


Fig. 5. Performance comparison on different approaches. (a) Mean sum channel capacity and mean fairness index per step. (b) Number of covert constraint violations per episode.

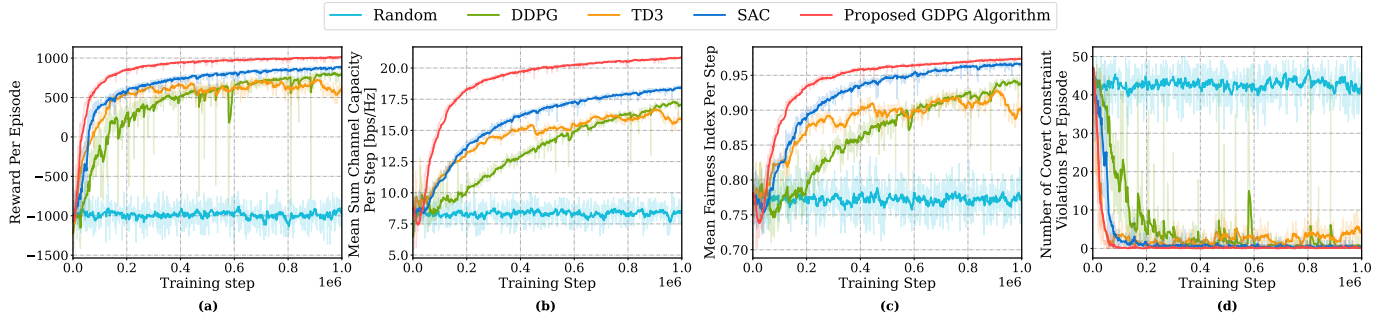


Fig. 6. Comparison of convergence curves of the proposed GDPG algorithm and some state-of-the-art DRL algorithms. (a) Reward per episode (b) Mean sum channel capacity per step. (c) Mean fairness index per step. (d) Number of covert constraint violations per episode.

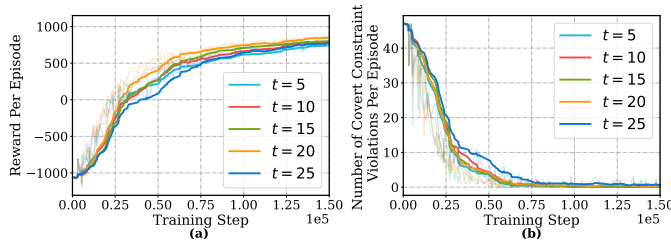


Fig. 7. Performance evaluations on different diffusion steps  $t$ . (a) Reward per episode. (b) Number of covert constraint violations per episode.

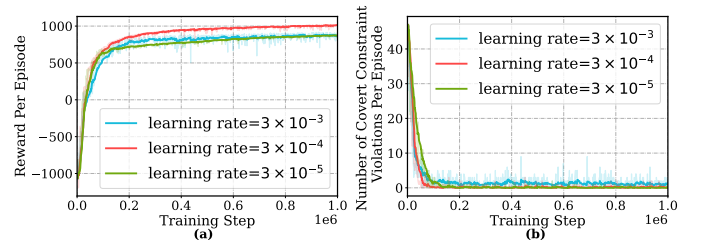


Fig. 8. Performance evaluations on different learning rates. (a) Reward per episode. (b) Number of covert constraint violations per episode.

Fig. 6(d) reveals the number of covert constraint violations per episode of the proposed GDPG algorithm in comparison to other algorithms. It is evident that the proposed GDPG algorithm effectively minimizes covert constraint violations while maintaining the lowest number of violations throughout the training phase. On the other hand, SAC results in a higher number of violations compared to the GDPG algorithm, especially in the early stages of training, which can be attributed to the entropy-driven exploration strategy that sometimes fails to maintain the strict covert constraints. Moreover, both DDPG and TD3 show similar trends, with DDPG experiencing a slightly higher number of violations than TD3. These algorithms struggle more than the GDPG algorithm in maintaining covert communication, likely due to their more limited exploration capabilities and lack of efficient optimization in complex environments.

3) *Impact of Different Diffusion Steps*: Figs. 7(a) and (b) show the performance of the proposed GDPG algorithm evaluated over different diffusion steps, specifically comparing the reward per episode and number of covert constraint violations per episode. To make the differences clearer, only the 150,000 training steps of the early training phase are shown. As can be seen in Fig. 7(a), regardless of the number of denoising steps, the algorithm demonstrates relatively stable progress in terms of rewards. This indicates that different denoising steps can effectively boost the reward accumulation, and the performance remains stable to a certain extent throughout the training process.

However, despite the stable performance in terms of rewards, the number of denoising steps is not always better when increased or decreased. From the results of Fig. 7(b), too many or few denoising steps can lead to slower convergence in terms

of the number of covert constraint violations per episode. This suggests that the optimal number of denoising steps should strike a balance between the stability and convergence speed. Moreover, the results in the figure indicate that  $t = 10$  might be the optimal choice, as it achieves both relatively stable reward improvement and avoids excessively slow convergence.

4) *Impact of Different Learning Rates*: Fig. 8(a) illustrates the impact of different learning rates on the convergence of reward per episode. It is observed that the reward increases rapidly at the initial training steps for all learning rates. Among them, the learning rate  $3 \times 10^{-4}$  provides the best balance between the convergence speed and stability, achieving the highest and most stable final reward. Conversely, the learning rate  $3 \times 10^{-3}$  exhibits faster initial learning but results in higher fluctuations, whereas a smaller learning rate leads to slow convergence with relatively lower performance.

Fig. 8(b) shows the number of covert constraint violations per episode for different learning rates during the training phase. Initially, all three cases exhibit a high number of violations, rapidly decreasing as training progresses. The learning rate  $3 \times 10^{-4}$  achieves the fastest and most stable convergence towards nearly zero violations. In contrast, the largest learning rate shows significant oscillations, and the smallest learning rate converges slowly. Thus, a moderate learning rate is preferred for effectively balancing the convergence speed and system constraint compliance.

5) *Impact of Different Covert Requirements*: In Fig. 9(a), the mean sum channel capacity and fairness index per step are shown for different covert requirements. As the covert requirement becomes more stringent (i.e.,  $\epsilon$  decreases), the mean sum channel capacity and mean fairness index per step slightly decrease. This indicates that enforcing higher

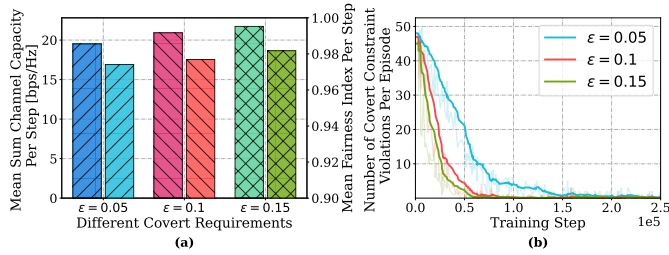


Fig. 9. Performance evaluations on different covert requirements  $\epsilon$ . (a) Mean sum channel capacity and mean fairness index per step. (b) Number of covert constraint violations per episode.

covertness reduces the available channel capacity and fairness, thereby highlighting the trade-off between ensuring the security and maximizing the communication performance.

Fig. 9(b) shows the number of covert constraint violations per episode for various covert requirements. As expected, a stricter covert requirement results in a higher number of covert constraint violations, particularly at the early stage of training. This is due to the difficulty of adhering to more stringent covert constraints, which leads to more violations during the exploration phase. However, as the training progresses, the algorithm increasingly adheres to the covert constraint with the number of violations gradually approaching zero.

In conclusion, the results show that while the GDPG algorithm can effectively maintain covertness with a relatively low number of violations, increasing the covert requirement introduces a trade-off between the sum channel capacity of all ground users, fairness among all ground users, and covertness of the considered system.

6) *Impact of Different AASTAR-RIS Sizes:* Fig. 10(a) shows the performance of the proposed GDPG algorithm with different AASTAR-RIS sizes. As the AASTAR-RIS size increases, the mean sum channel capacity per step gradually improves. Specifically, larger configurations, such as  $4 \times 4$  and  $5 \times 4$ , outperform smaller ones like  $1 \times 4$  and  $2 \times 4$ . This improvement occurs because larger AASTAR-RIS sizes have more transmission and reflection elements, which results in the enhanced signal amplification and reconfiguration capabilities, thereby leading to better communication performance. Moreover, the mean fairness index per step shows a similar trend. Specifically, larger AASTAR-RIS sizes provide better fairness, which suggests that the larger configurations help

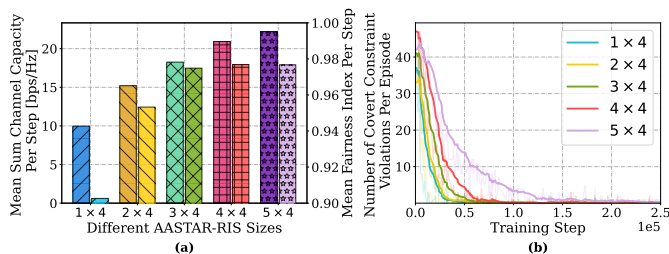


Fig. 10. Performance evaluations on different AASTAR-RIS sizes  $M_x \times M_y$ . (a) Mean sum channel capacity and mean fairness index per step. (b) Number of covert constraint violations per episode.

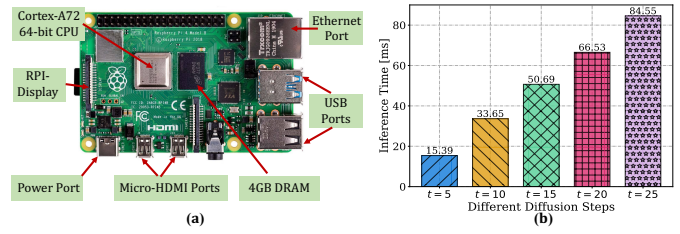


Fig. 11. Practicality test. (a) Raspberry Pi 4 Model B test platform. (b) Inference time evaluations on different diffusion steps  $t$ .

balance the communication capacity among multiple users more effectively. However, the performance gains become less pronounced as the size increases, which indicates that the optimal configuration may depend on a balance between the sum channel capacity of all users, fairness among all users and computational complexity.

Fig. 10(b) presents the number of covert constraint violations per episode during the early training phase for different AASTAR-RIS sizes. Specifically, smaller AASTAR-RIS sizes, such as  $1 \times 4$ , result in fewer covert constraint violations earlier in the training process compared to larger sizes like  $4 \times 4$  and  $5 \times 4$ . This happens because smaller configurations introduce less complexity, thereby allowing the algorithm to adapt more quickly and meet the covert communication requirements. While the larger AASTAR-RIS sizes provide higher channel capacity, they also introduce more complexity in satisfying the covert constraints, which results in slower convergence during the early stages of training. Therefore, smaller AASTAR-RIS sizes enable faster convergence with fewer covert constraint violations, while larger sizes require more time to optimize communication parameters and fully satisfy the covert requirements.

7) *Practicality Implementation:* We conduct some preliminary experiments to demonstrate the feasibility of our approach. Specifically, we utilize a Raspberry Pi 4 Model B, a widely used platform in UAVs and other LAP systems [35], for the experimental implementation, and the specific information is shown in Fig. 11(a). Moreover, Fig. 11(b) presents the inference time of the proposed GDPG algorithm evaluated over different diffusion steps. As can be seen, the inference time linearly increases as the number of denoising steps increases. This trend highlights that the inference time of the proposed GDPG algorithm remains within an acceptable hundred milliseconds. In conclusion, selecting the suitable number of denoising steps depends on finding the appropriate balance between exploration and inference time.

## VI. CONCLUSION

This paper has investigated a novel AASTAR-RIS assisted satellite-terrestrial covert communication scheme to confront a ground Warden. To achieve better communication performance and greater fairness among ground users while ensuring covertness, we have derived the covert constraint and formulated the ASCCOP to maximize the sum channel capacity of all ground users by jointly optimizing the trajectory and active beamforming of the AASTAR-RIS. To deal with the

long-term optimization problem, we have reformulated it into the framework of DRL and proposed a GDPG algorithm that leverages the GDM as policy representation to produce multimodal actions and adopts the action gradient method to improve the GDM-based policy. The simulation results have demonstrated the effectiveness of our approach over some different approaches. Moreover, we have also verified the robustness of the GDPG algorithm under different environment and algorithm parameters. In addition, the inference time of the GDPG algorithm on the Raspberry Pi has illustrated the practicality of the proposed approach. In future work, we will further study the combination implementation of LEO satellites and AASTAR-RIS to improve covertness performance.

## REFERENCES

- [1] S. Mahboob and L. Liu, "Revolutionizing future connectivity: A contemporary survey on AI-empowered satellite-based non-terrestrial networks in 6G," *IEEE Commun. Surv. Tutorials*, vol. 26, no. 2, pp. 1279–1321, 2nd Quart., 2024.
- [2] A. Al-Hourani, "On the probability of Line-of-Sight in urban environments," *IEEE Wirel. Commun. Lett.*, vol. 9, no. 8, pp. 1178–1181, Aug. 2020.
- [3] J. Li, G. Sun, Q. Wu, S. Liang, J. Wang, D. Niyato, and D. I. Kim, "Aerial secure collaborative communications under eavesdropper collusion in low-altitude economy: A generative swarm intelligent approach," *arXiv preprint arXiv:2503.00721*, Mar. 2025, doi: 10.48550/arXiv.2503.00721.
- [4] Y. Ding, Q. Zhang, W. Lu, N. Zhao, A. Nallanathan, X. Wang, and X. Yang, "Collaborative communication and computation for secure UAV-enabled MEC against active aerial eavesdropping," *IEEE Trans. Wirel. Commun.*, vol. 23, no. 11, pp. 15915–15929, Nov. 2024.
- [5] J. Li, G. Sun, Q. Wu, S. Liang, P. Wang, and D. Niyato, "Two-way aerial secure communications via distributed collaborative beamforming under eavesdropper collusion," in *Proc. IEEE Conf. Comput. Commun. (INFOCOM)*, Vancouver, Canada, May 20–23, 2024, pp. 331–340.
- [6] X. Chen, J. An, Z. Xiong, C. Xing, N. Zhao, F. R. Yu, and A. Nallanathan, "Covert communications: A comprehensive survey," *IEEE Commun. Surv. Tutorials*, vol. 25, no. 2, pp. 1173–1198, 2nd Quart., 2023.
- [7] C. Wang, X. Chen, J. An, Z. Xiong, C. Xing, N. Zhao, and D. Niyato, "Covert communication assisted by UAV-IRS," *IEEE Trans. Commun.*, vol. 71, no. 1, pp. 357–369, Jan. 2023.
- [8] L. Zhang, Z. Chen, C. Jiang, and L. Yin, "Covert communication in ultra-dense LEO satellite systems with interference uncertainty," in *Proc. IEEE Int. Conf. Commun. (ICC)*, Denver, CO, USA, Jun. 9–13 2024, pp. 1255–1260.
- [9] H. Jia, Y. Wang, W. Wu, and J. Yuan, "Robust transmission design for covert satellite communication systems with dual-CSI uncertainty," *IEEE Internet Things J.*, Early Access, 2025, doi:10.1109/JIOT.2025.3550098.
- [10] Z. Wu, H. Shuai, R. Liu, K. Guo, and S. Zhu, "Performance analysis of covert communication based on integrated satellite multiple terrestrial relay networks," in *Proc. 2022 IEEE 8th Int. Conf. Comput. Commun. (ICCC)*, Chengdu, China, Dec. 9–12 2022, pp. 380–385.
- [11] D. Song, Z. Yang, G. Pan, S. Wang, and J. An, "RIS-assisted covert transmission in satellite-terrestrial communication systems," *IEEE Internet Things J.*, vol. 10, no. 22, pp. 19415–19426, Nov. 2023.
- [12] Z. Guo, R. Sun, J. He, Y. Shen, and X. Jiang, "Covert communication in satellite-terrestrial systems with a full-duplex receiver," in *Proc. 2024 Int. Conf. Satell. Internet (SAT-NET)*, Xi'an City, China, Oct. 25–27, 2024, pp. 72–77.
- [13] H. Yu, J. Yu, J. Liu, Y. Li, N. Ye, K. Yang, and J. An, "Covert satellite communication over overt channel: A randomized gaussian signalling approach," *IEEE Trans. Aerosp. Electron. Syst.*, Early Access, 2024, doi:10.1109/TAES.2024.3475994.
- [14] K. Feng, T. Zhou, T. Xu, X. Chen, H. Hu, and C. Wu, "Reconfigurable intelligent surface-assisted multisatellite cooperative downlink beamforming," *IEEE Internet Things J.*, vol. 11, no. 13, pp. 23222–23235, Jul. 2024.
- [15] P. Hui, L. Guan, Z. Li, C. Li, W. Gao, and H. Zhang, "Covert communication in ultra-dense LEO satellite systems with interference uncertainty," in *Proc. IEEE Int. Conf. Commun. (ICC)*, Denver, CO, USA, Jun. 9–13 2024, pp. 1974–1979.
- [16] Y. Cao, Z. Guo, Q. Miao, R. Sun, J. He, and X. Li, "Minimization of age of information for satellite-terrestrial covert communication with a full-duplex receiver," in *Proc. Int. Conf. Networking Network Appl. (NaNA)*, Yinchuan City, China, Aug. 9–12, 2024, pp. 242–246.
- [17] W. D. Lukito, W. Xiang, P. Lai, P. Cheng, C. Liu, K. Yu, and X. Zhu, "Integrated STAR-RIS and UAV for satellite IoT communications: An energy-efficient approach," *IEEE Internet Things J.*, Early Access, 2024, doi: 10.1109/JIOT.2024.3472019.
- [18] X. Mu, Y. Liu, L. Guo, J. Lin, and R. Schober, "Simultaneously transmitting and reflecting (STAR) RIS aided wireless communications," *IEEE Trans. Wirel. Commun.*, vol. 21, no. 5, pp. 3083–3098, May 2022.
- [19] Z. Zheng, W. Jing, Z. Lu, Q. Wu, H. Zhang, and D. Gesbert, "Cooperative multi-satellite and multi-RIS beamforming: Enhancing LEO SatCom and mitigating LEO-GEO intersystem interference," *IEEE J. Sel. Areas Commun.*, vol. 43, no. 1, pp. 279–296, Jan. 2025.
- [20] Q. Wang, S. Guo, C. Wu, C. Xing, N. Zhao, D. Niyato, and G. K. Karagiannidis, "STAR-RIS aided covert communication in UAV air-ground networks," *IEEE J. Sel. Areas Commun.*, vol. 43, no. 1, pp. 245–259, Jan. 2025.
- [21] H. Lu, Y. Zeng, S. Jin, and R. Zhang, "Aerial intelligent reflecting surface: Joint placement and passive beamforming design with 3D beam flattening," *IEEE Trans. Wirel. Commun.*, vol. 20, no. 7, pp. 4128–4143, Jul. 2021.
- [22] J. Zhang, W. Wang, Y. Gao, W. Lu, N. Zhao, and D. Niyato, "Robust covert multicasting aided by STAR-RIS with hardware impairment," *IEEE Trans. Wirel. Commun.*, vol. 23, no. 11, pp. 16172–16186, Nov. 2024.
- [23] A. B. Sediq, R. H. Gohary, R. Schoenen, and H. Yanikomeroglu, "Optimal tradeoff between sum-rate efficiency and Jain's fairness index in resource allocation," *IEEE Trans. Wirel. Commun.*, vol. 12, no. 7, pp. 3496–3509, Jul. 2013.
- [24] X. Li, X. Du, N. Zhao, and X. Wang, "Computing over the sky: Joint UAV trajectory and task offloading scheme based on optimization-embedding multi-agent deep reinforcement learning," *IEEE Trans. Commun.*, vol. 72, no. 3, pp. 1355–1369, Mar. 2024.
- [25] J. Li, G. Sun, Q. Wu, D. Niyato, J. Kang, A. Jamalipour, and V. C. M. Leung, "Collaborative ground-space communications via evolutionary multi-objective deep reinforcement learning," *IEEE J. Sel. Areas Commun.*, vol. 42, no. 12, pp. 3395–3411, Dec. 2024.
- [26] M. Yi, X. Wang, J. Liu, Y. Zhang, and R. Hou, "Meta-reinforcement learning for timely and energy-efficient data collection in solar-powered UAV-assisted IoT networks," *IEEE Trans. Commun.*, Early Access, 2025, doi: 10.1109/TCOMM.2025.3543185.
- [27] D. Silver, G. Lever, N. Heess, T. Degris, D. Wierstra, and M. A. Riedmiller, "Deterministic policy gradient algorithms," in *Proc. 31th Int. Conf. Mach. Learn. (ICML)*, Beijing, China, Jun. 21–25 2014, pp. 387–395.
- [28] Z. Wang, J. J. Hunt, and M. Zhou, "Diffusion policies as an expressive policy class for offline reinforcement learning," in *Proc. 11th Int. Conf. Learn. Representations (ICLR)*, Kigali, Rwanda, May 1–5, 2023, pp. 1–17.
- [29] L. Yang, Z. Huang, F. Lei, Y. Zhong, Y. Yang, C. Fang, S. Wen, B. Zhou, and Z. Lin, "Policy representation via diffusion probability model for reinforcement learning," *arXiv preprint arXiv:2305.13122*, May 2023, doi: 10.48550/arXiv.2305.13122.
- [30] C. Zhang, G. Sun, J. Li, Q. Wu, J. Wang, D. Niyato, and Y. Liu, "Multi-objective aerial collaborative secure communication optimization via generative diffusion model-enabled deep reinforcement learning," *IEEE Trans. Mob. Comput.*, vol. 24, no. 4, pp. 3041–3058, Apr. 2025.
- [31] P. Dhariwal and A. Q. Nichol, "Diffusion models beat GANs on image synthesis," in *Proc. Adv. Neural Inf. Process. Syst. 2021 (NIPS)*, virtual, Dec. 6–14 2021, pp. 8780–8794.
- [32] S. Fujimoto, H. van Hoof, and D. Meger, "Addressing function approximation error in actor-critic methods," in *Proc. 35th Int. Conf. Mach. Learn. (ICML)*, Stockholm, Sweden, Jul. 10–15, 2018, pp. 1582–1591.
- [33] T. Haarnoja, A. Zhou, K. Hartikainen, G. Tucker, S. Ha, J. Tan, V. Kumar, H. Zhu, A. Gupta, P. Abbeel, and S. Levine, "Soft actor-critic algorithms and applications," *arXiv preprint arXiv:1812.05905*, Dec. 2018, doi:10.48550/arXiv.1812.05905.
- [34] D. Misra, "Mish: A self regularized non-monotonic neural activation function," *arXiv preprint arXiv:1908.08681*, Aug. 2019, doi:10.48550/arXiv.1908.08681.
- [35] A. N. Wilson, A. Kumar, A. Jha, and L. R. Kenkeramaddi, "Embedded sensors communication technologies computing platforms and machine learning for UAVs: A review," *IEEE Sensors J.*, vol. 22, no. 3, pp. 1807–1826, Feb. 2022.